CFD Comparisons with Updated NASA Juncture Flow Data

Abstract for AIAA SciTech Forum
January 11 – 15, 2021, Nashville, TN

C. L. Rumsey, N. N. Ahmad, J.-R. Carlson[*],
M. A. Kegerise, D. H. Neuhart, J. A. Hannon, L. N. Jenkins, C.-S. Yao, P. Balakumar[†],
S. M. Bartram[‡]
NASA Langley Research Center, Hampton, VA 23681
T. H. Pulliam[§]
NASA Ames Research Center, Moffett Field, CA 94035
P. R. Spalart[¶]
Boeing Commercial Airplanes, Seattle, WA 98124

I. Introduction

The NASA Juncture Flow (JF) experiment [1–3] was designed to be a "CFD validation" experiment of a wing-fuselage junction flow that experiences separation. The first set of tests [1], conducted in 2017-2018, provided high-quality mean and turbulence flowfield data from laser doppler velocimetry (LDV) measurements taken through windows on the fuselage in the near-corner region. These data are also available on the NASA Langley Turbulence Modeling Resource website [4].

Several Reynolds-averaged Navier-Stokes (RANS) CFD efforts have been conducted to date, comparing predictions with the experiment [5–10]. These efforts, involving several different turbulence models, have included grid-resolution studies (to ascertain the influence of numerical discretization errors on quantities of interest) as well as free-air versus in-tunnel studies (to ascertain the influence of wind tunnel walls). Other CFD efforts have included scale-resolving methods [11–14]. At AIAA Aviation 2020, additional special sessions are being held, including more than ten papers making CFD comparisons with the existing JF experimental data.

In early 2020, the same JF configuration was retested in the NASA Langley Research Center 14- by 22-Foot Subsonic Tunnel (14x22). The second test objectives were:

1. Repeats of some lines of LDV data for verification and uncertainty quantification
2. Fill in new data regions on the wing with LDV, including some "planes" (lines of data making a grid pattern)
3. Acquire LDV data at an additional angle of attack of 7.5 deg
4. Acquire flowfield velocity and Reynolds stress data with 3-component particle image velocimetry (PIV) in $x =$ constant planes over the wing trailing edge region at several angles of attack
   (a) Include some locations and conditions also examined by LDV
   (b) Provide a more complete picture of the JF flowfield in the juncture region

[*]Research Scientist, Computational AeroSciences Branch, Mail Stop 128.
[†]Aerospace Engineer, Flow Physics and Control Branch, Mail Stop 170.
[‡]Equipment Specialist, Advanced Measurement and Data Systems Branch, Mail Stop 493.
[§]Retired Senior Research Scientist, Computational Aerosciences Branch, Mail Stop 258-2.
[¶]Boeing Senior Technical Fellow, MS 0R-221.

5. Repeat model pressure measurements and investigate specific regions identified from the last test
6. Repeat oil flow at several angles of attack, including looks at both the wing and fuselage near the wing-fuselage junction
7. Obtain tunnel wall pressure data
8. Obtain tunnel wall rake boundary layer data on three walls
9. Repeat laser scan of assembled model, and Geographic Information System (GIS) scans of model, mast, and sting positioning in the tunnel
10. Document the transition behavior on the leading edge extension

With the additional quantitative flowfield data from the second test, the goal of the current paper is to (1) summarize new findings from the experiment, and (2) make comparisons between CFD and the updated experiment.

II. Preliminary Results

At this time, the 2020 experimental data are still being processed. However, they will be included in the final paper. Here, we show preliminary comparisons between CFD and experiment. All results are for a Reynolds number (based on crank chord) of $Re = 2.4 \times 10^6$ and Mach number of $M = 0.189$. The JF wing and part of its fuselage (with surface colored by pressure contours) are shown in Fig. 1(a). The focus of the joint CFD and experimental effort is the prediction of a small region of separated corner flow, whose size is a function of angle of attack. This separated region is indicated in the figure with a blue contour line near the wing trailing edge.

For the CFD, FUN3D [15] was employed on a semispan free-air grid, run fully turbulent with SA-RC [16, 17] as the baseline model in conjunction with a modified version of QCR2013 [18], termed QCR2020 [19], which will be fully described in the final paper. The grids from Rumsey et al. [8] were employed for this study. The unstructured fine grid was demonstrated to be sufficiently fine in the earlier study outside of the separation region, so it was used for all results shown here.

Sample plots demonstrating the effect of grid for the SA-RC-QCR2020 model are shown in Fig. 1 at $\alpha = 5^\circ$, along a specific line in the junction corner. The fine (F) grid used 161 million grid points and the medium (M) grid used 39 million grid points. As the figure shows, there was only a minor influence of grid on the velocity and Reynolds stress profiles, which was significantly smaller than the differences between CFD and experiment. These small differences, combined with consistent results at other locations as well as from a different code (OVERFLOW) in ref. [8], provided confidence that the discretization errors on the current unstructured fine grid were small enough for the purpose of evaluating turbulence model effectiveness leading into the separated region.

At this location deep in the wing junction upstream of separation, the CFD performed reasonably well for the mean flow (velocity profiles), slightly overpredicting the u-velocity component, but capturing its shape. There were significant differences in the turbulent normal stress components. In particular, the $\langle u'u' \rangle$ component was underpredicted. This was expected, because most turbulence models tend to underpredict the peak in this value very close to walls, and this profile lies right alongside (only 1 mm away from) the fuselage. However, turbulence models can perform well even when their normal Reynolds stress predictions are grossly inaccurate because their influence in the Navier-Stokes equations tends to be very small. On the other hand, second order derivatives in the spread between the normal stresses, and particularly between the $\langle v'v' \rangle$ and $\langle w'w' \rangle$ components for a flow aligned with the x-direction, are known to be important for sustaining a "stress-induced vortex" deep in corner regions [20]. This vortex is believed to have a significant effect on the corner separation location further downstream [8, 21]. Here, the CFD results captured the shapes and relative spread between the $\langle v'v' \rangle$ and $\langle w'w' \rangle$ components reasonably well. For the turbulent shear stress components, the CFD yielded excellent results for $\langle u'v' \rangle$ and $\langle v'w' \rangle$, and did very well for the $\langle u'w' \rangle$ component very near the wall ($z < 20$ mm).

CFD contours of the v component of velocity in the $x = 2747.6$ mm plane using three different turbulence models are shown along with preliminary LDV results in Fig. 2. At this location upstream of separation on the wing, the LDV results (Fig. 2(a)) suggest the presence of the stress-induced vortex in the corner region (the small positive v-velocity region points into the fuselage wall on the right, indicative of counterclockwise-rotating flow located just below the vortex [8]). The CFD with SA-RC-QCR2020 (Fig. 2(b)) produces a stronger effect than SA-RC-QCR2013 (Fig. 2(c)), in better agreement with the experiment. Without QCR, SA-RC does not produce a stress-induced vortex at all (Fig. 2(d)), and results in a corner separation that is far too large [8]. The presence of the corner vortex acts to delay the onset of separation; and the stronger the vortex, the more separation is delayed.

Figure 3 compares oil flow photographs from the experiment with CFD surface-restricted streamlines at three different angles of attack. Note that the photographs were not taken from exactly the same location, whereas the CFD views in the figures are identical. Qualitatively, the CFD captured the size and overall trend of increasing separation size with angle of attack. The final paper will include additional quantitative measures, along with surface pressure comparisons and comparisons between both LDV and PIV flowfield data in specific planes both upstream of and within the separated region.

References

[1]Kegerise, M. A., Neuhart, D. H., "An Experimental Investigation of a Wing-Fuselage Junction Model in the NASA Langley 14- by 22-Foot Subsonic Tunnel," NASA/TM-2019-220286, June 2019, https://ntrs.nasa.gov/archive/nasa/casi.ntrs.nasa.gov/20190027403.pdf.

[2]Rumsey, C. L., Neuhart, D. H., and Kegerise, M. A., "The NASA Juncture Flow Experiment: Goals, Progress, and Preliminary Testing," AIAA Paper 2016–1557, January, 2016, doi: https://doi.org/10.2514/6.2016-1557.

[3]Rumsey, C. L., "The NASA Juncture Flow Test as a Model for Effective CFD/Experimental Collaboration," AIAA Paper 2018-3319, June 2018, doi: https://doi.org/10.2514/6.2018-3319.

[4]Rumsey, C. L., "NASA Langley Turbulence Modeling Resource Website," https://turbmodels.larc.nasa.gov, Accessed: 2020-02-21.

[5]Rumsey, C. L., Carlson, J.-R., Hannon, J. A., Jenkins, L. N., Bartram, S. M., Pulliam, T. H., Lee, H. C., "Boundary Condition Study for the Juncture Flow Experiment in the NASA Langley 14x22-Foot Subsonic Wind Tunnel," AIAA Paper 2017-4126, June 2017, doi: https://doi.org/10.2514/6.2017-4126.

[6]Rumsey, C. L., Carlson, J.-R., Ahmad, N. N., "FUN3D Juncture Flow Computations Compared with Experimental Data," AIAA Paper 2019-0079, January 2019, doi: https://doi.org/10.2514/6.2019-0079.

[7]Lee, H. C., Pulliam, T. H., "OVERFLOW Juncture Flow Computations Compared with Experimental Data," AIAA Paper 2019-0080, January 2019, doi: https://doi.org/10.2514/6.2019-0080.

[8]Rumsey, C. L., Lee, H. C., Pulliam, T. H., "Reynolds-Averaged Navier-Stokes Computations of the NASA Juncture Flow Model Using FUN3D and OVERFLOW," AIAA Paper 2020-1304, January 2020, doi: https://doi.org/10.2514/6.2020-1304.

[9]Abdol-Hamid, K. S., Ahmad, N. N., Carlson, J.-R., Biedron, R. T., "Juncture Flow Computations using kL-Based Turbulence Models," AIAA Paper 2020-1305, January 2020, doi: https://doi.org/10.2514/6.2020-1305.

[10]Eisfeld, B., Togiti, V., Braun, S., Sturmer, A., "Reynolds-Stress Model Computations of the NASA Juncture Flow Experiment," AIAA Paper 2020-1306, January 2020, doi: https://doi.org/10.2514/6.2020-1306.

[11]Iyer, P. S. and Malik, M. R., "Wall-modeled LES of the NASA Juncture Flow Experiment," AIAA Paper 2020-1307, January 2020, doi: https://doi.org/10.2514/6.2020-1307.

[12]Lozano-Duran, A., Moin, P., and Bose, S. T., "Prediction of trailing edge separation on the NASA Juncture Flow using wall-modeled LES," AIAA Paper 2020-1776, January 2020, doi: https://doi.org/10.2514/6.2020-1776 and https://doi.org/10.2514/6.2020-1776.c1.

[13]Balin, R., Wright, J., Patterson, J., Farnsworth, J. A., Evans, J. A., Lakhani, R., Spalart, P., and Jansen, K. E., "Hybrid Turbulence Model Computations of the NASA Juncture Flow Model Using PHASTA," AIAA Paper 2020-1777, January 2020, doi: https://doi.org/10.2514/6.2020-1777.

[14]Duda, B. M. and Laskowski, G. M., "Lattice-Boltzmann Very Large Eddy Simulations of the NASA Juncture Flow Model," AIAA Paper 2020-1778, January 2020, doi: https://doi.org/10.2514/6.2020-1778.

[15]"FUN3D Users Manual," https://fun3d.larc.nasa.gov, Accessed: 2020-02-19.

[16]Spalart, P. R. and Allmaras, S. R., "A One-Equation Turbulence Model for Aerodynamic Flows," *Recherche Aerospatiale*, Vol. 1, 1994, pp. 5–21.

[17]Shur, M. L., Strelets, M. K., Travin, A. K., Spalart, P. R., "Turbulence Modeling in Rotating and Curved Channels: Assessing the Spalart-Shur Correction," *AIAA Journal*, Vol. 38, No. 5, 2000, pp. 784–792, doi: https://doi.org/10.2514/2.1058.

[18]Mani, M., Babcock, D. A., Winkler, C. M., and Spalart, P. R., "Predictions of a Supersonic Turbulent Flow in a Square Duct," AIAA Paper 2013-0860, January 2013, doi: https://doi.org/10.2514/6.2013-0860.

[19]Rumsey, C. L., Carlson, J.-R., Pulliam, T. H., and Spalart, P. R., "Improvements to the Quadratic Constitutive Relation Based on NASA Juncture Flow Data," manuscript submitted to AIAA Journal.

[20]Perkins, H. J., "The Formation of Streamwise Vorticity in Turbulent Flow," *Journal of Fluid Mechanics*, Vol. 44, Part 4, 1970, pp. 721–740, doi: https://doi.org/10.1017/S0022112070002112.

[21]Bordji, M., Gand, F., Deck, S., and Brunet, V., "Investigation of a Nonlinear Reynolds-Averaged Navier-Stokes Closure for Corner Flows," *AIAA Journal*, Vol. 54, No. 2, 2016, pp. 386–398, doi: https://doi.org/10.2514/1.J054313.

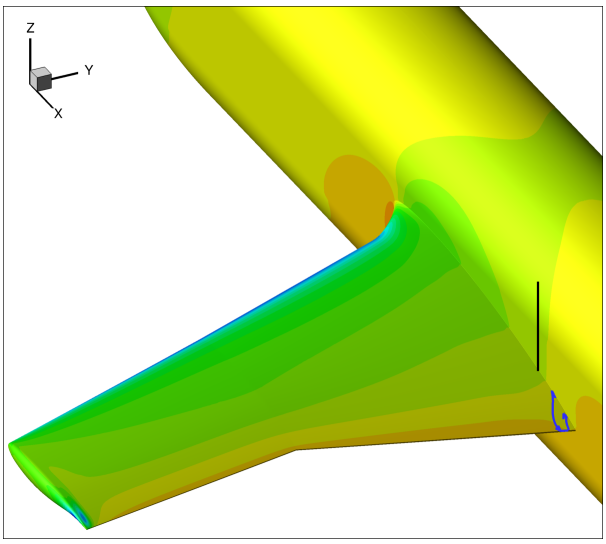

(a) Location of profile (approx. separation size shown for reference)

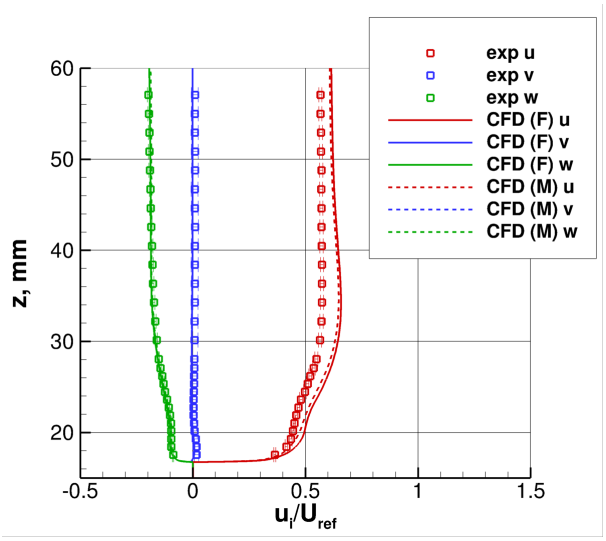

(b) Velocity profiles

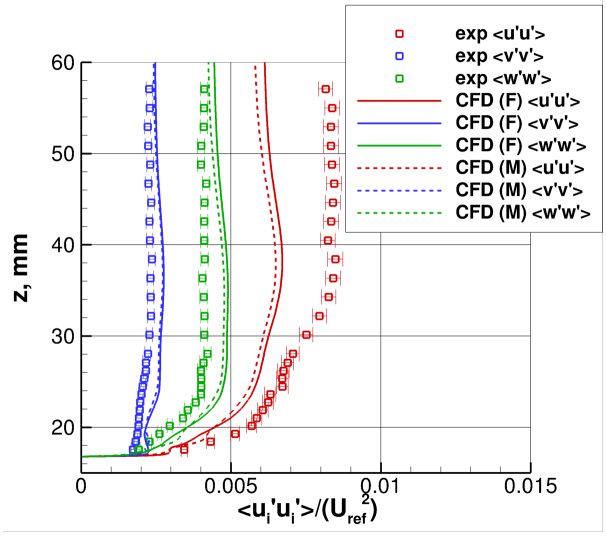

(c) Turbulent normal stress profiles

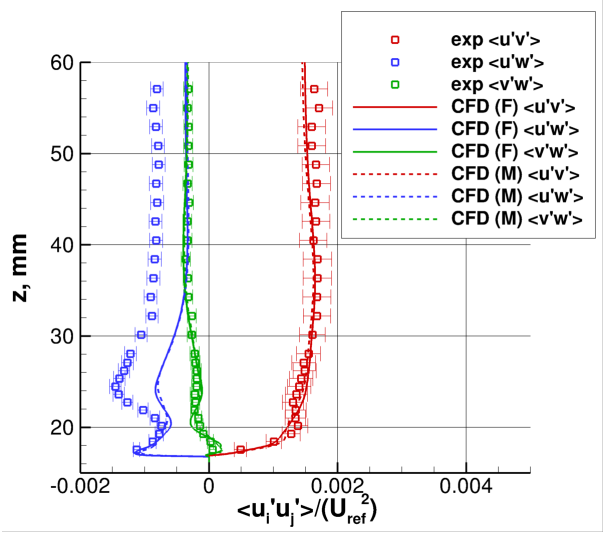

(d) Turbulent shear stress profiles

Figure 1. Effect of grid on profiles from CFD results upstream of separation on wing (approx. 1 mm from fuselage, inside its boundary layer), $x = 2747.6$ **mm,** $y = -237.1$ **mm,** $\alpha = 5°$**.**

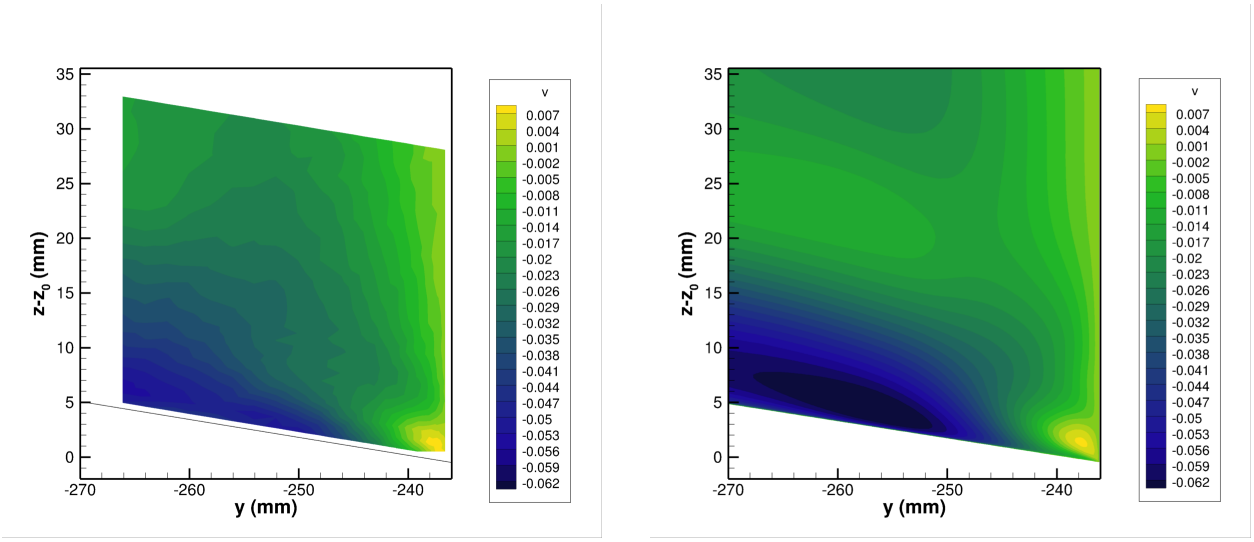

(a) experiment, LDV

(b) CFD, SA-RC-QCR2020 model

(c) CFD, SA-RC-QCR2013 model

(d) CFD, SA-RC model

Figure 2. Profiles of v/U_{ref} in $x = 2747.6$ mm plane, upstream of separation on wing, $\alpha = 5°$.

(a) Photograph from the experiment, $\alpha = -2.5^\circ$

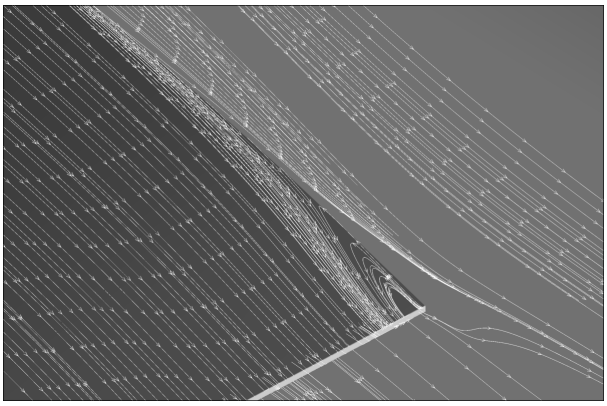

(b) CFD at $\alpha = -2.5^\circ$

(c) Photograph from the experiment, $\alpha = 5^\circ$

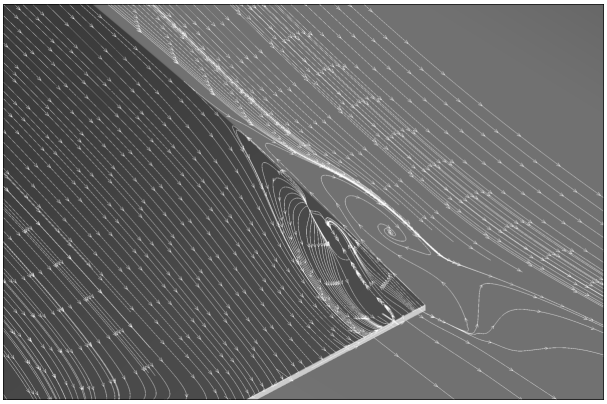

(d) CFD at $\alpha = 5^\circ$

(e) Photograph from the experiment, $\alpha = 7.5^\circ$

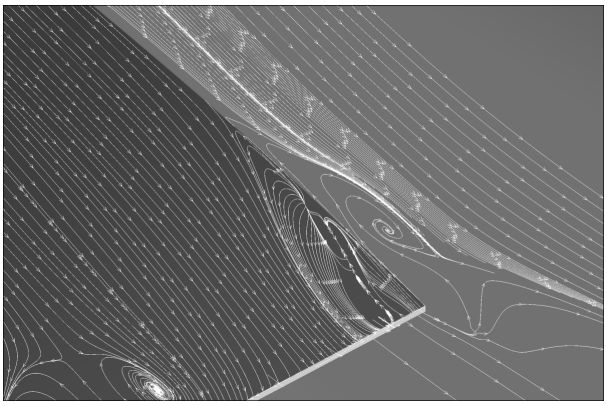

(f) CFD at $\alpha = 7.5^\circ$

Figure 3. JF change in corner separation size with angle of attack.